IEEE Access
Multidisciplinary ⋮ Rapid Review ⋮ Open Access Journal

Received 13 March 2024, accepted 11 April 2024, date of publication 19 April 2024, date of current version 3 May 2024.
Digital Object Identifier 10.1109/ACCESS.2024.3391385

RESEARCH ARTICLE

Electromagnetic Characterization of Hyperconducting Aluminum Litz Wires at Cryogenic Temperatures

HONGYE ZHANG[1], (Member, IEEE), MATTEO F. IACCHETTI[1,2], (Senior Member, IEEE), ALEXANDER C. SMITH[1], (Senior Member, IEEE), PAUL M. TUOHY[1], CHARALAMPOS D. MANOLOPOULOS[3], ALEXANDRU-VLAD RUSU[1], AND VICENTE CLIMENTE-ALARCON[3], (Senior Member, IEEE)
[1]Department of Electrical and Electronic Engineering, The University of Manchester, M13 9PL Manchester, U.K.
[2]Department of Energy, Politecnico di Milano, 20156 Milan, Italy
[3]GKN Aerospace, BS34 6FB Bristol, U.K.

Corresponding authors: Alexander C. Smith (sandy.smith@manchester.ac.uk) and Matteo F. Iacchetti (matteo.iacchetti@manchester.ac.uk)

This work was supported by the Aerospace Technology Institute/INNOVATE U.K. & GKN Aerospace funded project "Hybrid Hydrogen & Electric Architecture (H2GEAR)."

ABSTRACT Cryogenic electric machines (CEMs) offer significant potential for highly power-dense and ultra-efficient net-zero aircraft. Aluminum (Al) displays superior conductivity to copper (Cu) at cryo-temperatures, making Al Litz wires an attractive option for CEM windings to minimize DC and eddy losses. However, accurately quantifying Al Litz wire losses remains challenging, particularly considering their unknown electromagnetic behavior at different cryo-temperatures and frequencies when embedded in iron cores. To address this, a specialized test setup was developed to measure the losses of two customized Al Litz coils, alongside a Cu Litz coil, under varying cryo-temperatures (25 to 77 K) and frequencies (50 to 1000 Hz). A numerical model was also developed using COMSOL, incorporating a temperature-dependent electrical conductivity and a homogenization model for Litz wires with rectangular cross-sections. The model was incorporated into an analytic design procedure to maximize the test-rig loss ratio within the tight space and maximum heat rejection constraints of the cryostat, to allow accurate loss separation. The experimental data aligns closely with the numerical simulations, enabling a comprehensive analysis of the loss characteristics of Al Litz wires. This study provides a detailed design methodology and serves as a valuable resource for developing CEMs for zero-emission electric aircraft.

INDEX TERMS Cryogenic electric machine, hyperconducting aluminum Litz wire, loss separation, test rig design, net-zero electric aircraft.

I. INTRODUCTION

This work was part of a large consortium project launched in 2020 to develop hydrogen technology and accelerate aerospace decarbonization to zero emissions [1]. One key objective of this project was to develop the world's first Hyperconducting electric propulsion motor for a subregional net-zero electric aircraft by exploiting high-purity aluminum (Al) Litz wires operating at cryo-temperatures.

The use of liquid hydrogen as an aviation fuel has led to increasing interest in cryogenic technologies for enhancing the performance of conductors [2] for cables, electric machines and drives [3], [4], [5], potentially leading to a significant reduction in conductor losses [6], [7]. Regarding the winding materials for cryogenic electric machines (CEMs), two types are commonly considered: superconducting

The associate editor coordinating the review of this manuscript and approving it for publication was R. K. Saket.

materials and hyperconducting materials. Superconducting materials can be classified into low-temperature superconductors (e.g., Nb3Sn, Nb3Al, and NbTi) and high-temperature superconductors (HTSs, e.g., REBCO, BSCCO, and MgB2) based on their critical temperatures [8]. HTSs are promising materials functioning at liquid hydrogen temperatures given their critical temperatures are above 20 K. While HTSs can substantially diminish DC loss in CEMs for hydrogen-powered aircraft [9], the persistent challenge lies in the significant AC loss observed in them [8], despite extensive research efforts on HTS electric machines using HTS tapes [10], [11]. Hyperconducting materials typically refer to highly pure, conductive metals exhibiting significantly reduced electrical resistivity at cryogenic temperatures, such as copper (Cu) and aluminum (Al). Zheng et al. designed a 200 krpm super-high speed cryogenic synchronous motor adopting a cryogenic permanent magnet rotor and Cu stator windings, both operating at 77 K [12]. Marignetti et al. constructed and tested a cryogenic tubular linear actuator and they found that the resistivity of the utilized Cu windings cooled by liquid nitrogen decreased by 84% compared to windings operating at room temperature [13]. Kim et al. fabricated a cryogenic induction motor exploiting Cu armature windings and Al bars, both submerged in liquified natural gas at -163°, with 88.8% efficiency at 37 kW rated output [14]. Although Cu is widely employed for electric machine windings due to its favorable electrical and thermal conductivities, high-purity Al operating at cryo-temperatures below 70 K provides better electrical and thermal conductivities and a reduction of machine mass [15]. Consequently, at cryo-temperatures, Al emerges as a promising material for CEM windings when acting as a hyperconductor (Al is actually a superconductor at $T < 1.2$ K). Scott et al. first proposed that hyperconducting Al is a promising candidate for field windings of high power density pulsed AC generators because of its high current-carrying capacity at 20 and 28 K and light weight [16]. Filusch et al. proposed a conceptual design of a hyperconducting synchronous machine using Al stator windings cooled by liquid hydrogen (20 K) for high-torque applications [17].

A Litz wire, comprising multiple insulated metal strands twisted or braided together, effectively mitigates high-frequency losses attributed to skin and proximity effects. As a result, Litz wires have gained traction in various power electronic applications, including power converters [18], [19], wireless power transfer systems [20], [21], electric motors, and generators [22], [23]. Given the high-frequency environment in the AC windings of CEMs and electric aircraft drives, Al Litz wires have the potential to address the persistent challenge of AC losses encountered with HTS tapes, while exhibiting relatively lower DC loss compared to Cu Litz wires at cryo-temperatures. The comprehensive understanding of the electromagnetic characteristics of Al Litz wires in CEMs however remains limited, owing to their relatively limited application in electric machines and power electronics, as well as the nascent stage of CEM development.

Different test rigs have been designed to characterize Litz wires. The DC and AC resistances of impregnated Litz wires with non-insulated Cu strands were specially studied by use of an iron stack that emulates the slots of an actual machine in [23]. However, the test rig in [23] is not applicable at cryo-temperatures because motorette coils do not effectively exploit the limited cryogenic space envelope of small cryostats and their free end-windings can induce eddy losses in the surrounding cryogenic test containment which then hinders accurate loss segregation. The proximity losses in Cu Litz wires were measured by a test bench composed of a soft ferrite core and Litz wire excitation coils in [24], which actually adopted the same approach as presented in [25]. In [25] a skin effect test rig was also introduced comprising a circular groove through a brass bar to form the inner conductor of a coaxial waveguide. However, the above-mentioned test rigs are all focused on room temperature measurements for Cu Litz wires. A cryogenic test rig has been recently proposed in [26] to study the proximity loss of different Cu and Al Litz wires; however, the temperature was confined at 77 K and only the proximity effect was investigated.

AC windings in electric machines are commonly embedded into slots in the magnetic core to provide support and shield them from the full working magnetic field. These coils however are still subjected to the lower density magnetic fields passing across the slots (slot leakage) [27]. To characterize the loss properties of Al Litz wires subjected to slot magnetic fields of varying frequencies over a range of cryogenic temperatures, a specialized AC test rig was developed, facilitating the separation of DC and eddy current losses in different Litz coils. Additionally, a finite element method (FEM)-based numerical model was developed, integrating a homogenized model for Litz wires that considers temperature-dependent electrical conductivity. By comparing the results from the numerical modeling and experimental tests, the efficacy of the developed numerical model for cryogenic Litz wires was validated, the functionality of the designed AC test rig was confirmed, and the loss characteristics of Al Litz wires operating at cryogenic temperatures within an electric machine slot environment were elucidated. This study is expected to serve as a valuable resource for the design of CEMs and cryogenic energy conversion systems.

This article is structured as follows: Section II outlines the analytical equations utilized for quantifying Litz wire losses and homogenization modeling of Litz wires. Section III details the development of the AC test rig employed for Litz wire loss separation. Section IV presents the numerical modeling and test results of different Litz wire samples at distinct cryogenic temperatures and frequencies. Finally, Section V draws the primary conclusions from the study.

II. LITZ WIRE AC LOSS FORMULATIONS

A. BACKGROUND

The losses generated in Litz wires are composed of two primary components: resistive loss (DC loss) and eddy current loss [28]. The resistive loss is caused by the DC resistance, which is independent of frequency; the eddy current loss is frequency dependent and comprises skin and proximity effects. The resistive loss, P_{DC}, is given by:

$$P_{DC} = I_{rms}^2 R_{DC} = \frac{4 I_{rms}^2 \rho l k_t}{N \pi d_s^2} \tag{1}$$

where I_{rms} is the effective AC transport current, R_{DC} represents the frequency-independent DC resistance of the Litz wire, ρ represents the electrical resistivity of the Litz strand, l is the axial length of the whole Litz wire, k_t refers to the twist factor of the Litz wire which accounts for the extended length of the individual strands as a result of the twist, N is the number of strands in the Litz wire, and d_s stands for the strand diameter.

A correctly chosen Litz wire should be able to minimize the skin effect, i.e., the strand diameter ought to be no higher than the skin depth, δ. Under the condition $d_s \leq \delta$, according to [26], the eddy current loss caused by the skin effect and proximity effect can be written as:

$$P_{eddy} = I_{rms}^2 R_{DC} \left[\frac{N(N-1)}{128} \left(\frac{d_s}{d_L}\right)^2 \left(\frac{d_s}{\delta}\right)^4 \right] + \frac{N l k_t}{16} \frac{(B_{rms} f_B)^2 \pi^3 d_s^4}{\rho} \tag{2}$$

where d_L is the diameter of the Litz wire, B_{rms} is the rms value of the external AC magnetic flux density, and f_B refers to the frequency of the external magnetic field. The skin depth, δ, is determined by:

$$\delta = \sqrt{\frac{\rho}{\pi f_C \mu}} \tag{3}$$

where f_C denotes the frequency of the AC transport current, and μ is the permeability of the Litz wire material.

For Litz wires that are made from linear magnetic materials, their total losses can be obtained by simply adding P_{DC} and P_{eddy} [29]. It should be pointed out that in practical applications, e.g., for armature windings in electric machines, the external magnetic field seen by each strand in the Litz is not evenly distributed and thus (2) cannot be directly utilized to quantify the eddy current loss (further information can be found in Discussion). In this case, the magnetic field distribution in the Litz wire needs to be determined and FEM based numerical modeling methods are commonly adopted.

B. NUMERICAL MODELING METHODOLOGY

Modelling a large number of individual strands of a Litz wire in a motor winding using FEM can be computationally very time-consuming, especially in the time domain: meshing of each thin single strand can generate an enormous number of degrees of freedom (DOFs). Homogenization methods for Litz wires in the frequency domain therefore provide a good alternative for fast computation of AC losses in complex winding arrangements [30], [31], [32]. These often involve the definition of a homogenized or "effective" conductivity and permeability of the winding region, as shown in Figure 1. Many proposed homogenization approaches require preliminary FEA analyses to tune the homogenized winding properties, which makes parametric sensitivity analyses of AC losses slow and cumbersome, especially for design optimization. A closed-form formulation for the effective homogenized complex conductivity and permeability of Litz regions filled with hexagonally packed round wires (see Figure 1) was proposed in [31], with:

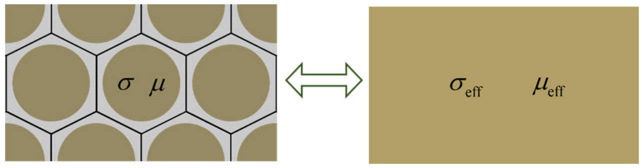

FIGURE 1. Diagram of the homogenization of the hexagonally packed Litz wire.

$$\sigma_{eff} = \frac{\sigma k_f}{\frac{\mu_0}{\mu_{fd}} + \frac{(1-c)}{c} j\Omega - \frac{1}{3}\frac{\mu_{eff}}{c\mu_0} j\Omega} \tag{4}$$

$$\mu_{eff} = (1-c)\mu_0 + c\mu_{fd} \tag{5}$$

where σ represents the electrical conductivity of the Litz material, k_f is the fill factor for the Litz conductors in the studied homogenization region, and μ_0 is the vacuum permeability. The constant c is the fill factor of the equivalent foil geometry:

$$c = \sqrt{\frac{2\sqrt{3}\, k_f}{\pi}} \tag{6}$$

Ω represents the non-dimensional frequency:

$$\Omega = \frac{\sqrt{3}\pi^2}{16} c f \sigma \mu_0 d_s^2 \tag{7}$$

and μ_{fd} refers to the frequency-dependent permeability of a single equivalent foil, defined by:

$$\mu_{fd} = \frac{\mu_0 \tanh\left(\sqrt{j\Omega}\right)}{\sqrt{j\Omega}} \tag{8}$$

Clearly, in the numerical model of a cryogenic hyperconducting winding, the temperature-dependent conductivity of Al Litz wires has to be considered. The temperature-dependent electrical resistivities $\rho(T)$ of Al and Cu are described by [33]:

$$\rho = \rho_0 + \rho_i + \rho_{i0} \tag{9}$$

where ρ_0 denotes the residual resistivity (the constant value of resistivity in the limit of zero temperature); ρ_i represents the intrinsic resistivity, which is characterized by electrons interacting with phonons, with $\rho_{i(T=273K)} = 24.8$ nΩ·m for Al and 15.4 nΩ·m for Cu; and ρ_{i0} refers to a deviation term [33]:

$$\rho_0 = \frac{\rho_{i(T=273K)}}{\text{RRR-1}} \tag{10}$$

$$\rho_i = \frac{P_1 T^{P_2}}{1 + P_1 P_3 T^{P_2+P_4} e^{-(P_5/T)^{P_6}}} + \rho_c \tag{11}$$

TABLE 1. Curve fitting parameters for the $\rho(T)$ curves of Al and Cu.

Parameters	Values	
	Cu	Al
P_1	1.1171×10^{-17}	0.9052×10^{-17}
P_2	4.49	4.551
P_3	3.841×10^{10}	5.173×10^{10}
P_4*	-1.14	-1.26
P_5	50	40
P_6	6.428	13.64
P_7	0.4531	0.7416

*The two curve-fitted values given in [33] missed the negative sign.

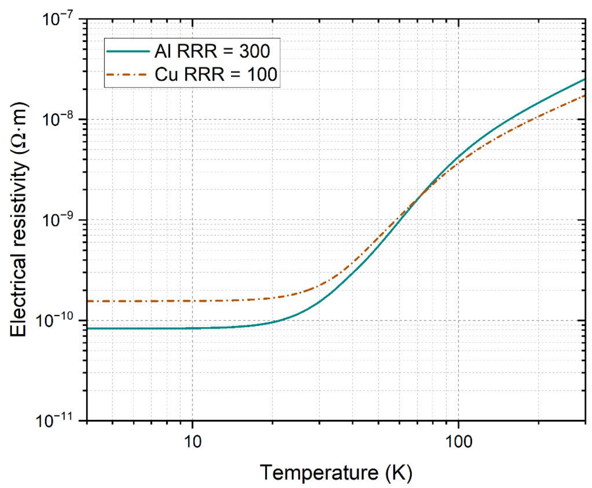

FIGURE 2. Electrical resistivities of Al with RRR = 300 and Cu with RRR = 100 in the temperature range of 4-300 K.

$$\rho_{i0} = \frac{P_7 \rho_i \rho_0}{\rho_i + \rho_0} \tag{12}$$

where ρ_c is included to account for the mathematical residual deviations in ρ_i. For Al and Cu, ρ_c has been taken as zero. RRR represents the Residual-Resistance Ratio. The RRR values for the Cu and Al Litz wires tested in this paper are 100 and 300 respectively and were determined by experimental measurements. Curve fitting parameters in (11)-(12) for the temperature variation of the resistivity of Al and Cu are shown in Table 1, and the $\rho(T)$ curves of the studied Al and Cu are shown in Figure 2. It can be seen that the chosen Al with RRR = 300 becomes more conductive than Cu with RRR = 100 at $T < 70$ K.

III. TEST RIG DESIGN AND MODELING

A. CONCEPT AND OPERATING PRINCIPLE

To evaluate the performance of Litz coils at cryo-temperatures in a representative environment, a test rig with a rectangular slot has been designed, as shown in Figure 3. The test rig is composed of a group of magnetic iron cores, a test Litz coil, and a Nylon support structure. This test rig was designed to provide a reasonable emulation of the magnetic slot-leakage field in a winding slot of an electrical machine and to correlate this to an analytic loss-density calculation model for the Litz wire [34], to allow validation. Compared to other rigs used at room temperature [23], [24], [25], the axisymmetric structure confines the field within the core to minimize eddy currents in the cryostat containment Cu bucket which would impede an accurate loss separation.

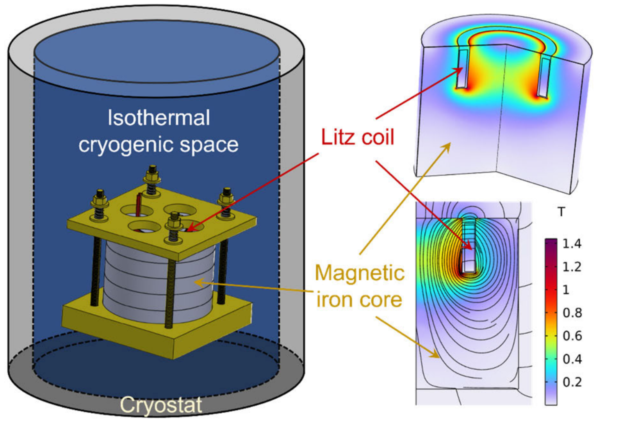

FIGURE 3. Diagram of the test rig in the cryostat.

The losses generated in the Litz coils are composed of DC and eddy current losses; however, it is challenging to directly measure them experimentally. To evaluate the loss performance of the Al Litz coils, their losses have to be separated from other losses produced in other parts of the test system. The Al Litz eddy current loss can be calculated as:

$$P_{\text{eddy,Al}} = P_{\text{rig,Al}} - P_{\text{core}} - P_{\text{DC,Al}} \tag{13}$$

where $P_{\text{rig,Al}}$ is the total losses generated in the test rig using Al Litz coils, P_{core} represents the iron core loss, and $P_{\text{DC,Al}}$ denotes the DC resistive loss of the Al Litz coil. This assumes there are no losses due to stray fields in the cryostat containment vessel – however, we believe these will be negligibly small.

The challenge of the experimental test therefore comes from the accurate determination of $P_{\text{rig,Al}}$, P_{core}, and $P_{\text{DC,Al}}$:

$P_{\text{rig,Al}}$– The total rig loss is the electrical active power directly measured at the coil terminals;

$P_{\text{DC,Al}}$ – The resistive loss of the tested Al Litz coil can be calculated based on (1), which requires the measurement of the DC resistance of the Litz coil at different temperatures;

P_{core} – The iron core loss is the most difficult to measure. It is separated here by a second test run under the same operating conditions and total slot current, by replacing the Al coil under test with one of the identical geometrical dimensions but made of Cu with much thinner strands thus reducing the Cu Litz eddy current loss to a negligible level. In this way, the core loss can be obtained by:

$$P_{\text{core}} = P_{\text{rig,Cu}} - P_{\text{DC,Cu}} \tag{14}$$

where $P_{\text{rig,Cu}}$ is the total test rig losses using the thin-stranded Cu Litz coil and $P_{\text{DC,Cu}}$ refers to the resistive loss of the Cu Litz coil. Equation (14) also requires the measurement of the DC resistance of the Cu Litz coil at different temperatures in order to quantify $P_{\text{DC,Cu}}$. It should be noted here that a

0.04mm diameter strand Cu Litz wire was adopted in the determination of P_{core}. This followed an assessment of the available strand diameters down to 0.01 mm to identify a suitable strand size that ensures the Litz eddy current loss is negligible.

B. CORE MATERIAL SELECTION

Somaloy® 700 was chosen as the iron core material because it has lower losses than Ferrite at LN_2 temperature (77 K) and low-moderate frequencies. It has the further advantage of an inherently higher saturation limit – approximately 1.5 T. In addition, an extensive set of experimental loss measurements for Somaloy® 700 can be found in [35] at different frequencies and magnetic flux density levels, although only at 77 K and room temperature. The frequency range tested varied from 50 Hz to 1 kHz, which aligned very well with the test rig specification. The experimental DC *B-H* curve for Somaloy® 700 at 77 K was found in [36] and it exhibited only a slight reduction in *B* mainly at low *H* values around 1000 A/m compared to room temperature. The outer diameter (OD) of the iron core was set to 120 mm based on the available Somaloy® core sizes from Höganäs AB.

C. DESIGN STRATEGY

The primary design variables are shown in Figure 4. In an ideal Litz wire, the macroscopic current density distribution (i.e., at the slot level) is uniform; and in the test rig shown in Figure 4, the slot-leakage magnetic field crossing the slot travels predominantly in the radial direction, with a near-zero axial component. By ignoring the radial variation of *B* caused by the axisymmetric geometry, the slot flux density has a triangular distribution with zero and maximum values at the slot bottom and mouth, respectively (see Figure 4). The peak value (in the time domain) of the maximum flux density (at slot mouth) is given by:

$$B_{pk,max} = \sqrt{2}\, k_{fill}\mu_0 h_s J_{rms} \tag{15}$$

where k_{fill}, h_s, and J_{rms} are the coil fill factor, coil/slot height (assuming that the coil fills the slot), and rms source current density (ratio between the rms value of the injected current and the slot cross-sectional area), respectively.

The slot leakage flux density in a CEM is typically below 0.4 T and thus the rig was designed for $B_{pk,max} = 0.4$ T. For a Litz wire strand fill factor of 0.44 and a turn packing factor of 0.85, $k_{fill} = 0.37$. J_{rms} was set to 20 A/mm^2. Therefore, based on (15), h_s was calculated as 30 mm.

A parametric, axisymmetric 2D numerical model was also established within COMSOL Multiphysics. The Litz wire coil region has adopted the homogenization model presented in Section II. The *B-H* curve data of the Somaloy® core have been taken from [36] (relevant to 77 K) due to a lack of available data at different temperatures. The cryostat containment vessel was fabricated from Electrolytic Tough-Pitch Cu and was modeled in order to assess any potential eddy losses due to field fringing: modeling results showed that the maximum Cu bucket loss is 0.5 W, which was assumed to be neglectable.

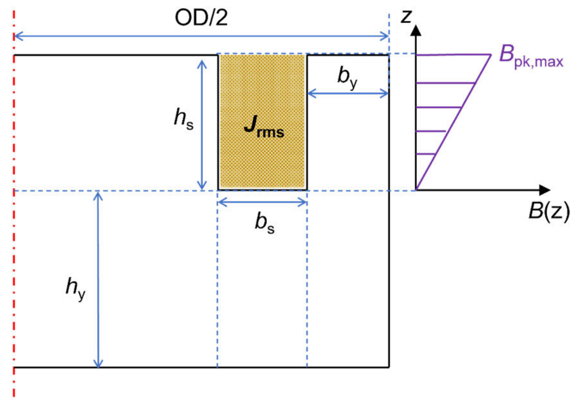

FIGURE 4. Test rig geometry, design variables, and slot-leakage flux density distribution.

The whole model was analyzed in the frequency domain, encompassing temperatures ranging from 20 to 100 K and frequencies varying from 50 to 1000 Hz.

A RRR-100 Cu Litz coil with 0.25 mm strands was selected for the optimization of the test rig. To facilitate accurate segregation of the measured Litz eddy current loss, it is sensible to maximize the Litz eddy current loss to total rig loss ratio, *ELR*, defined by:

$$ELR = \frac{P_{eddy}}{P_{rig}} \tag{16}$$

A multi-dimensional parametric sweep over the remaining free variables b_s, b_y, and h_y was run using the COMSOL model to calculate the loss breakdown, the *ELR* from (16), and the apparent power *S* with a single-turn homogenized coil. The constraints for the parametric sweep include:

1) The maximum output power of the lab power supply was 10 kVA, and thus the apparent power of the test rig $S <$ 10 kVA;

2) To allow reliable Litz wire eddy loss segregation, *ELR* should be maximized - from previous experience on Litz wire loss characterization [34], the minimum *ELR* requirement was 12%;

3) By assuming short-duration ($<$ 200 ms) tests within the quasi-adiabatic test region (the test rig is surrounded by a vacuum space to minimize heat exchange with the surroundings), the total test rig loss at 77 K was below 150 W.

Figure 5 shows the *ELR* trend versus b_s and b_y. The orange region violates Constraint 1), the blue region violates Constraint 3), and the red region violates both Constraints 1) and 3). As a result, the optimal design was chosen with: b_s = 7 mm, b_y = 25 mm, h_y = 70 mm, and S = 8.51 kVA. In this case, ELR = 16% which complies well with Constrain 2).

The required Litz coil geometry and wire parameters were determined based on the power supply V and A constraints: supply rms voltage $V_{rms} \leq 300$ V and rms current $I_{rms} \leq 80$ A. By assuming that, at the target frequency and cryo-temperature, the Joule losses of the tested Litz coil are negligible compared to the reactive power demand, the

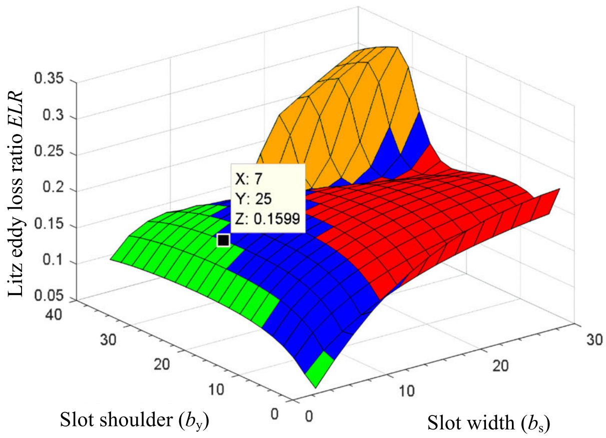

FIGURE 5. ELR trend for a RRR-100 0.25 mm strand Cu Litz coil as a function of dimensions bs and by, with unfeasible regions (orange, blue and red).

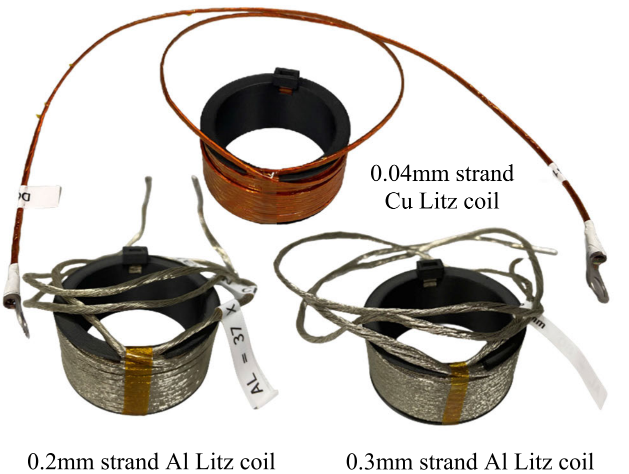

FIGURE 6. Photos of the tested Al and Cu Litz coil samples.

voltage and current constraints translate into the following inequalities involving the number of turns N_t:

$$\frac{1}{I_{max}}\sqrt{\frac{S}{X_1}} \leq N_t \leq \frac{V_{max}}{\sqrt{S X_1}} \tag{17}$$

where X_1 is the single-turn reactance with the maximum $X_1 = 3.56$ mΩ at 1 kHz. Finally, the coil turns $N_t = 40$ (4 layers ×10 turns per layer) was chosen in order to integrate the rectangular-cross-sectional dimensions of the Litz wire: 1.5 mm × 3 mm. Three bespoke Litz wires with this cross section and different strand diameter were manufactured and investigated: a 0.2mm and a 0.3mm strand diameter Al Litz wire with 80 and 37 strands respectively, as well as a 0.04mm strand diameter Cu Litz wire with 1500 strands. The completed coils were wound onto 3D-printed polyamide formers, as shown in Figure 6.

The twist factor provided by the supplier is k_t =1.04. The average diameter for the three Litz coils is 62.7 mm. The cross-sectional areas for the 0.2mm and 0.3mm strand diameter Al Litz coils and the Cu Litz coil are 178.12 mm^2, 165.27 mm^2, and 168 mm^2, respectively.

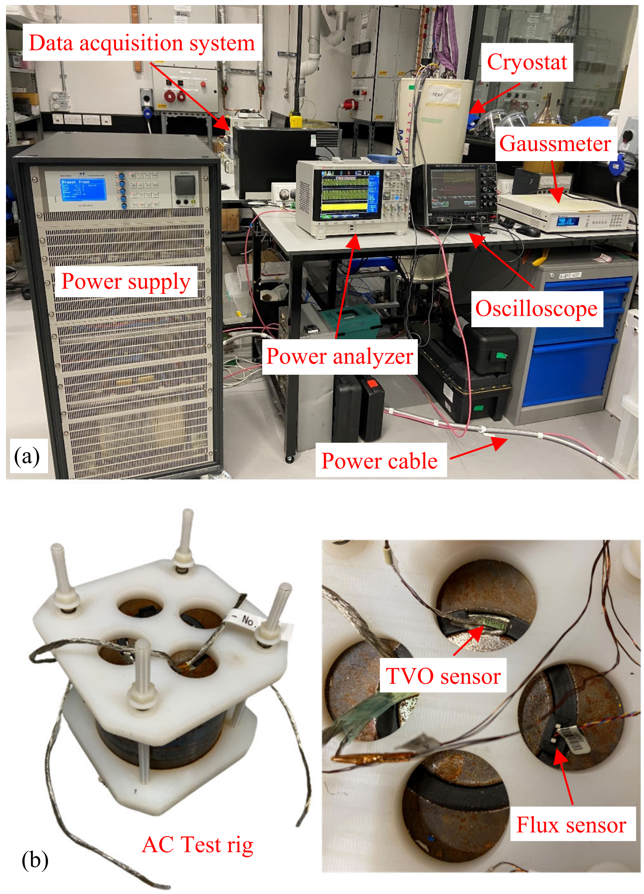

FIGURE 7. Photo of the entire Litz coil test system. (a) Measurement system; (b) AC test rig.

D. MEASUREMENT SYSTEM

A photo of the experimental AC test rig and measurement system is shown in Figure 7. A 10 kVA, 300 Vrms, 80 Arms single-phase linear power supply with a maximum output frequency of 1 kHz was used to provide DC and AC currents at different frequencies. A Keysight PA2203A IntegraVision Power Analyzer was used to measure the total test rig losses. A cryogenic Hall flux sensor was positioned within the slot to measure the leakage flux density – despite the limited frequency range of up to 400 Hz of the Gaussmeter, it served to validate the test rig design, but the measured flux density was not required to determine the Litz coil losses. Cryogenic temperature sensors were used to measure the temperature variation of the Litz coils. The temperature sensors with 1.8 K - 300 K operating range were attached to the Litz coils on the top of the last turn near the slot opening.

It should be noted that the resistances of the Litz coils becomes negligible compared to their reactances at cryo-temperatures, especially at higher frequencies. As a result, the whole electric circuit becomes inductance-dominant and thus there will be a significant current/voltage inrush transient in the Litz coils when the supply is switched on. The long settling time will inevitably cause measurement errors. To attenuate the impact of the transient inrush current/voltage, a 1Ω resistor was initially added in series with the Litz coil on test to minimize the inrush transients. The power analyzer was also configured to record current and voltage signals following the transient phase. A LeCroy 44Xi-A Oscilloscope with 400 MHz bandwidth and 5 GS/s sample rate was connected to the power analyzer and used to send a trigger signal to the power analyzer when the transient current and voltage inrush passed.

IV. RESULTS AND ANALYSES

This study involved temperature variations from 25 to 77 K (across 8 temperature points) and AC current frequencies ranging between 50 and 1000 Hz (covering 6 frequency points), with a fixed applied current of 40 Arms. Initially, the operating temperature was set using the cryostat, followed by tests at different frequencies. Each test at a specific temperature and frequency required an hour-long interval for the temperature to stabilize before the next test. As a result, achieving data points at each preset temperature requires approximately 6 hours (including DC tests), and to encompass all frequencies, the entire process for each Litz coil test extended over 8 working days.

A. IRON LOSS SEPARATION

To separate the different loss components, described by (13) and (14), the DC losses of the tested coils were needed. The DC resistances of the three tested coils were measured first, as shown in Figure 8. This shows that the DC resistances of the two Al Litz coils were lower than the Cu coil with the same coil length because the Al wires (RRR = 300) have a higher conductivity at cryogenic temperatures than the 0.04 mm strand Cu wire (RRR = 100) and also have a higher conductor area due to a better fill factor with the lower strand number. In addition, the DC resistance of all three coils decreases significantly with decreasing temperature, which confirms that at cryo-temperatures the DC resistive loss of Cu/Al windings can be greatly reduced. Based on (14), the core loss was separated by taking the difference of the total test rig loss and the DC loss of the 0.04mm diameter strand Litz coil. The resulting iron core losses at different temperatures and frequencies and presented in Figure 9.

It can be seen from Figure 9 that for different frequencies, the iron loss has a close to linear correlation with the temperature, and thus linear equations were used to curve-fit the experimental data in Figure 9. It is not hard to understand that the iron loss would decrease with increasing temperature because the electrical conductivity of the iron material decreases with increasing temperature and thus less eddy current losses will be generated. However, for a fixed temperature, the increase in iron loss is non-linear with increasing frequency as predicted by the classical Bertotti model [37] which separates the iron loss into hysteresis loss ($\propto f$), eddy current loss ($\propto f^2$), and excess loss ($\propto f^{1.5}$).

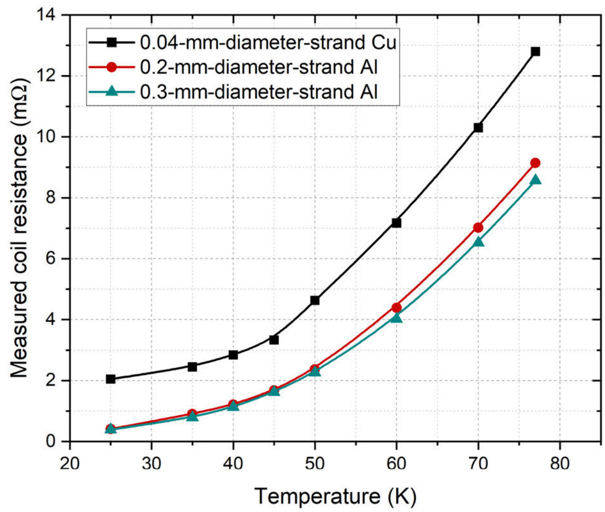

FIGURE 8. Measured resistances of different Litz wire coils at different temperatures.

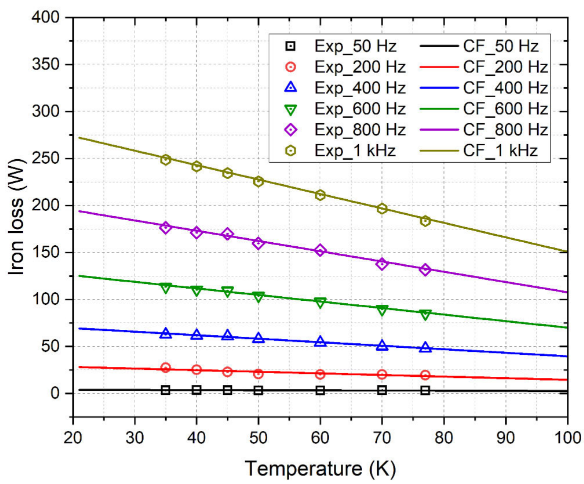

FIGURE 9. Measured and curve-fit iron losses at different temperatures and frequencies. Exp – experiment; CF – curve fitting.

B. LITZ COIL EDDY CURRENT LOSS SEPARATION

The simulated and measured total rig losses for the 0.3mm strand Al Litz coil are shown together in Figure 10; and in general, the correlation between the measured and modelled losses is good. The separated Litz eddy current losses for the 0.3mm strand Litz coil are shown in Figure 11. The total rig losses decrease with increasing temperature because the Al Litz coil eddy loss and iron loss dominate (especially at high frequencies) within the studied temperature range, both of which become less significant as temperature increases. It should be noted that the simulated results use the iron losses calculated from the curve-fit equations shown in Figure 9 because the iron properties, e.g., the temperature-dependent electrical conductivity at cryo-temperatures are unknown. The measured data however appears lower than the modeled results, especially at lower temperatures and higher frequencies. One potential reason would be that the discrepancy is due to the temperature increase during the test measurement:

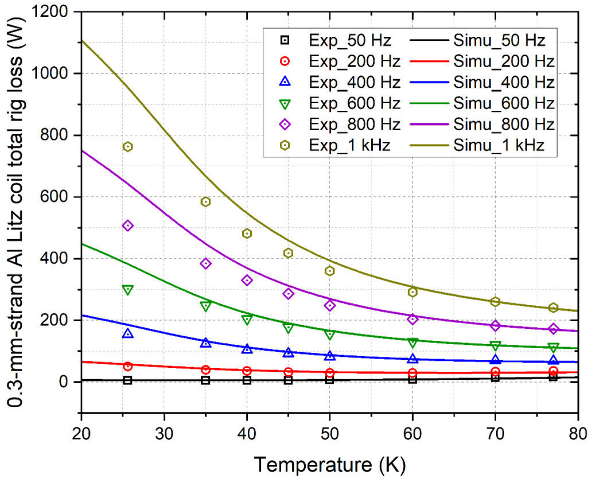

FIGURE 10. **Measured and simulated total rig losses for the 0.3mm diameter Al Litz coil. Exp – experiment; Simu – simulation. In the simulation, RRR = 300 for the tested Al Litz wire.**

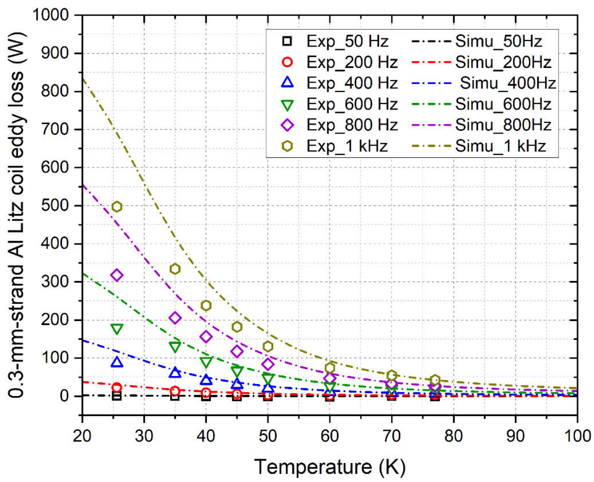

FIGURE 11. **Separated Litz eddy current losses for the 0.3mm diameter Al Litz coil. Exp – experiment; Simu – simulation. In the simulation, RRR = 300 for the tested Al Litz wire.**

1) The temperatures for the experimental data are the nominal values, namely the starting temperature of the AC test; but in reality, the temperature of the Litz coil will rise due to heating caused by the AC power dissipation; 2) In addition, to measure the test rig losses accurately it is important to wait for the transient inrush period caused by the circuit inductance in the order of tens of milliseconds to decay to steady-state conditions and during this period the temperature is also expected to increase.

It can be seen from Figure 11 that the eddy current loss increases quickly in a non-linear way with both decreasing temperature and increasing frequency. The impact of the temperature shift discussed above also pulls through to Figure 11 as well. However despite a good agreement between measurement and simulation at higher temperatures and lower frequencies, the separated eddy current losses of the 0.3mm Litz coil appear lower than the modeling results at higher frequencies and lower temperatures.

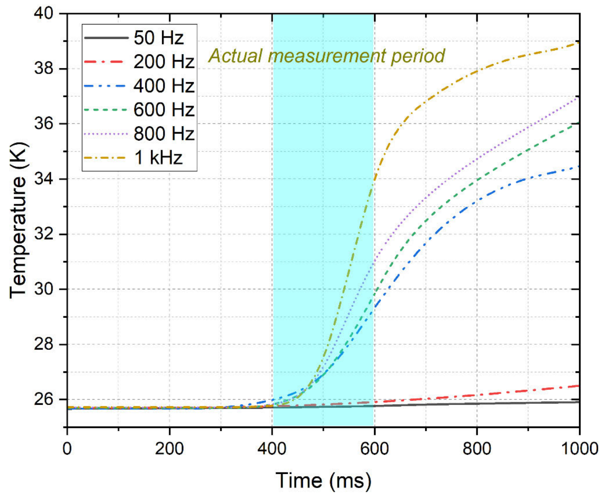

FIGURE 12. **Variation of temperature during the test measurement of the 0.2mm diameter strand Al Litz coil at different frequencies, with the starting temperature 25.6 K.**

To investigate the potential temperature shift effect during measurements, another test was conducted on the 0.2mm Al Litz coil. For this test, the temperature variation during the test measurement duration, 200 ms, was recorded with a sampling step of 100 ms and this allowed the loss data to be correlated to the true measured temperature of the test coil. Taking the nominal temperature 25.6 K as an example, the temperature variation of the tested Litz coil during measurements at different frequencies is demonstrated in Figure 12. It can be seen that the coil temperature keeps increasing during the test measurement (the power supply was turned on at approximately $t = 400$ ms and turned off at around $t = 600$ ms) and here we adopted the temperature at the end of the actual measurement period to reflect the true coil temperature.

The experimental and simulated results are presented in Figures. 13 and 14. It can be seen that the loss data with the corrected temperatures now agree very well with the numerical modeling results, which would validate the assumption that the data deviations in Figures 10 and 11 are caused by the measurement temperature shift. In addition, by comparing the loss data at nominal and corrected temperatures, it can be concluded that the temperature shift is more pronounced at lower temperatures and higher frequencies because of two potential reasons: first, a higher frequency and a lower temperature (meaning a higher electrical conductivity) together lead to higher eddy current losses in the Litz coil, as shown in Figure 14, which can lead to more heating and thus a more significant temperature shift; secondly, the specific heat of Al decreases with lower temperatures, and thus a higher temperature variation is expected at lower temperatures for the same amount of heat generated in the Al coils. From Figure 14 it can be seen that the separated Litz eddy current losses from experiments are also in good agreement with simulation, which has not only confirmed the validity of the developed numerical model incorporating the homogenized Litz wires in this paper but also verified the loss separation methodology proposed in Section III.

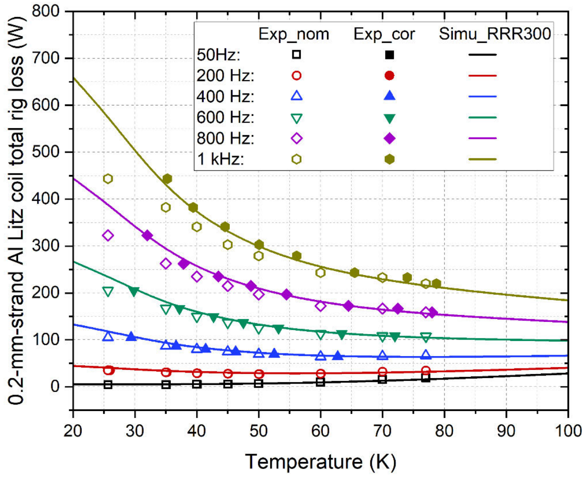

FIGURE 13. Measured and simulated total rig losses for the 0.2mm wire. The hollow points represent the measurement data at nominal temperatures, the solid points refer to the loss data at corrected temperatures after considering the temperature shift effect, and the solid lines are the modeled results with RRR = 300 for the tested Al Litz wire. Nom – nominal; cor – corrected.

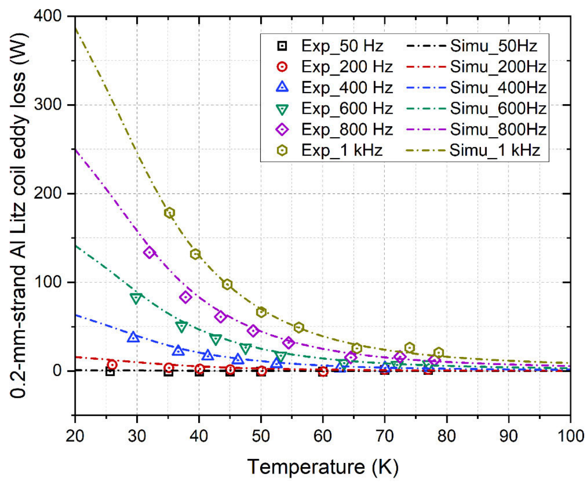

FIGURE 14. Separated Litz eddy current losses for the 0.2mm wire. Exp – experiment; Simu – simulation. In simulation, RRR = 300 for the tested Al Litz wire.

By comparing Figures 11 and 14, it can be seen that the Litz coil eddy current losses can be significantly mitigated by reducing the Litz strand diameter, as predicted by (2). Taking 1 kHz and 20 K as an example, the Litz eddy current loss drops from 830 W to 380 W by replacing 0.3mm with 0.2mm diameter strands, corresponding to an approximately 54% loss reduction. However, thinner Litz wires can be more fragile and susceptible to damage during handling and installation, which can affect the overall robustness and reliability of the windings; additionally, thinner Litz wires also result in increased manufacturing complexity and higher costs. In practical design work for CEMs and cryogenic energy conversion systems, the choice of Litz wires should not only consider the loss reduction effect but also the specific system design, cryogenic cooling budget and method, mechanical strength, as well as cost-effectiveness.

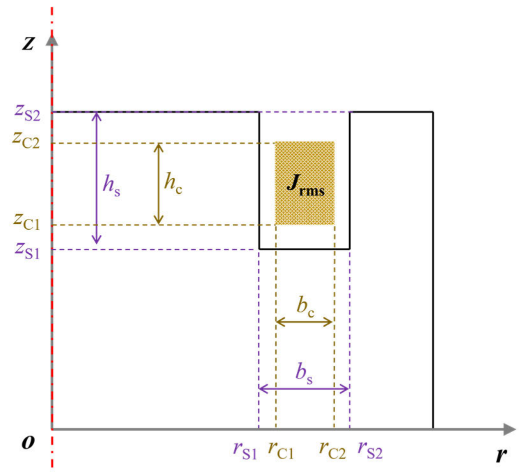

FIGURE 15. Cross-sectional diagram of the test rig in the cylindrical coordinate system.

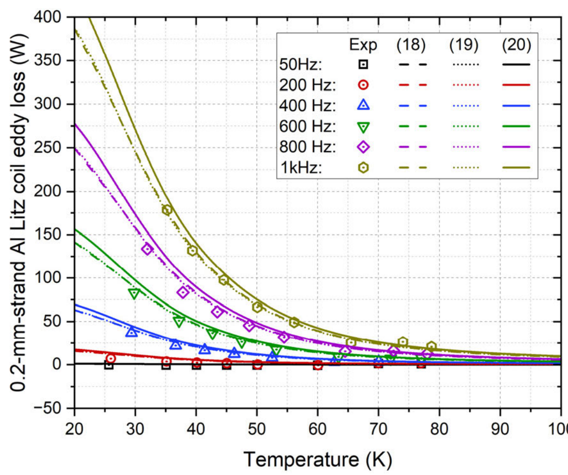

FIGURE 16. Eddy current losses of the 0.2mm diameter strand Litz coil calculated by different approaches, compared to the measured data.

V. DISCUSSION

The simulated Litz coil eddy losses presented above have been calculated by integrating the COMSOL built-in magnetic power loss density, Q_{ml}, over the coil volume:

$$P_{\mathrm{eddy}} = \iiint_V Q_{\mathrm{ml}} dV = \frac{1}{2}\iiint_V Re\left(i\omega B \cdot \mathbf{H}^*\right) dV \quad (18)$$

where ω is the angular frequency and i is the imaginary unit.

In this paper, the studied frequency is relatively low (no higher than 1 kHz) and at most of the studied temperatures, we have $d_{\mathrm{s}} \leq \delta$ [see (3)]: the skin effect of Litz wires can be neglected. In this case, based on (2), the eddy current loss can also be calculated by:

$$P_{\mathrm{eddy}} \approx \iiint_V \frac{\left(B_{\mathrm{pk}}\omega r_s\right)^2}{8\rho} dV = \frac{Nlk_{\mathrm{t}}}{16}\frac{\left(B_{\mathrm{rms}} f_{\mathrm{B}}\right)^2 \pi^3 d_{\mathrm{s}}^4}{\rho} \quad (19)$$

where B_{pk} is the peak flux density amplitude, r_{s} is the radius of the Litz strand, N denotes the number of strands per Litz turn, and l is the total length of the Litz wire in the coil.

Taking it one step further: the Litz coils here were situated in a regular rectangular slot and thus the magnetic field distribution across the Litz coil cross sections, $B_{\mathrm{pk}}(r,z)$, can be quantified analytically. Based on (19), it can be inferred that the eddy current loss can be calculated analytically if an average B_{rms}^2 across the whole Litz coil cross section can be derived:

$$P_{\mathrm{eddy}} \approx \frac{Nlk_{\mathrm{t}}f_{\mathrm{B}}^2\pi^3 d_{\mathrm{s}}^4}{16}\frac{}{\rho}\overline{B_{\mathrm{rms}}^2} \tag{20}$$

Let us consider a more general case where the Litz coil does not fully fill the slot, as shown in Figure 15: r_{C1} and r_{C2} represent the inner and outer radius of the Litz coil; z_{C1} and z_{C2} denote the coil bottom and top coordinates; r_{S1} and r_{S2} refer to the inner and outer radius of the slot; and z_{S1} and z_{S2} stand for the slot bottom and top coordinates. The slot leakage field lines are still assumed to be parallel to the r-axis. Based on Ampère's circuital law we have

$$\int_{r_{\mathrm{S1}}}^{r_{\mathrm{S2}}} B_{\mathrm{pk}}(r,z)dr = \mu_0 J_{\mathrm{pk}} k_{\mathrm{f,c}} b_{\mathrm{c}}\left(z - z_{\mathrm{C1}}\right) \tag{21}$$

where b_{c} and h_{c} are the coil width and height, respectively; $r_{\mathrm{S1}} \le r \le r_{\mathrm{S2}}$ and $z_{\mathrm{C1}} \le z \le z_{\mathrm{C2}}$. Notably, here the Litz coil fill factor, $\mathrm{k}_{\mathrm{f,c}}$, should be calculated by

$$k_{\mathrm{f,c}} = \frac{\pi r_{\mathrm{s}}^2 N N_{\mathrm{t}}}{b_{\mathrm{c}} h_{\mathrm{c}}} \tag{22}$$

where $\mathrm{N_t}$ is the number of turns in the Litz coil.

According to Gauss's law $\nabla \cdot \mathbf{B} = 0$, along the r-axis the magnetic flux density should decrease inversely with increasing radius, namely

$$B_{\mathrm{pk}}(r,z) = B_{\mathrm{pk}}(r_{\mathrm{S1}},z)\frac{r_{\mathrm{S1}}}{r} \tag{23}$$

Consequently, (21) - (23) give

$$B_{\mathrm{pk}}(r,z) = \frac{\mu_0 J_{\mathrm{pk}} k_{\mathrm{f,c}} b_{\mathrm{c}}}{\log\left(r_{\mathrm{S2}}/r_{\mathrm{S1}}\right)}\frac{z - z_{\mathrm{C1}}}{r} \tag{24}$$

Then, $\overline{B_{\mathrm{rms}}^2}$ can be derived as

$$\overline{B_{\mathrm{rms}}^2} = \frac{\int_{z_{\mathrm{C1}}}^{z_{\mathrm{C2}}}\int_{r_{\mathrm{C1}}}^{r_{\mathrm{C2}}} B_{\mathrm{pk}}^2(r,z)drdz}{2b_{\mathrm{C}}h_{\mathrm{C}}} = \frac{1}{3r_{\mathrm{C1}}r_{\mathrm{C2}}}\left[\frac{\mu_0 k_{\mathrm{f,c}} b_{\mathrm{c}} h_{\mathrm{c}}}{\log\left(r_{\mathrm{S2}}/r_{\mathrm{S1}}\right)}\right]^2 J_{rms}^2 \tag{25}$$

Taking the 0.2mm strand diameter Litz coil as an example, the eddy current losses calculated by (18), (19), and (20) using the average flux density squared from (25) have been depicted together in Figure 16. Here, $r_{\mathrm{C1}} = 28.4$ mm, $r_{\mathrm{C2}} = 34.3$ mm, $z_{\mathrm{C1}} = 30.3$ mm, $z_{\mathrm{C2}} = 60.8$ mm, $r_{\mathrm{S1}} = 27.0$ mm, $r_{\mathrm{S2}} = 34.9$ mm, $z_{\mathrm{S1}} = 29.5$ mm, and $z_{\mathrm{S2}} = 61.5$ mm. $J_{\mathrm{rms}} = 15.92$ A/mm^2 for the injected current 40 Arms. It can be seen that the calculated eddy current losses by (18) and (19) agree closely with each other for all the studied frequencies and temperatures, which further confirms that the skin effect for the 0.2mm diameter strand Litz coil is neglectable in the frequency range up to 1 kHz at varying temperature from 20 to 100 K. As a comparison, in general, the analytical results calculated by (20) are in good accordance with (18) and (19), though (20) overestimated the eddy current losses by approximately 9.8% compared to (18) and (19). It should be noted that the $B_{\mathrm{pk}}(r,z)$ surface was assumed to linearly vary in the z direction to facilitate the derivation of the formulae, as described by (21) and (24). However, in reality, this linear variation trend does not hold in the regions near the slot opening. Nevertheless, (20) serves as a useful analytical method allowing for quickly quantifying eddy current losses in Litz coils and cross-checking modeling and experimental results.

VI. CONCLUSION

Through numerical modeling and experimental measurements, this research has conducted a comprehensive analysis of the loss behavior of Al Litz coils with varying strand diameters, when subjected to slot magnetic fields typical of electric machines with frequencies ranging from 50 to 1000 Hz, across different cryogenic temperatures from 25 to 77 K. The numerical model has integrated a homogenization model for Litz wires with rectangular cross-sections considering the temperature-dependent electrical conductivity of Al and Cu. The development of the bespoke cryogenic AC test rig has been meticulously delineated, involving a loss separation methodology for characterizing the eddy current losses of different Al Litz coils, and iron loss. The Al Litz wires have been shown to function as a hyperconductor with enhanced electrical conductivity at cryo-temperatures. The eddy current loss of Al Litz wires increases in a non-linear way with both decreasing temperatures and increasing frequencies; however, the eddy current loss can be effectively mitigated by reducing the Litz strand size. The experiments also provided ancillary information such as the iron losses in Somaloy® 700 cores, with a linear increase in the iron loss with decreasing temperature and a non-linear rise with increasing frequency, suggesting a dominant eddy current loss due to the increased core electrical conductivity at lower cryogenic temperatures.

This paper serves as a robust modeling and experimental framework for quantifying the Litz wire losses at cryo-temperatures. The data presented herein are being directly utilized in the H2GEAR project for designing a novel ultra-efficient cryogenic electric motor for zero-emission electric aircraft, and the resultant conclusions offer valuable insights for informing the design of cryogenic electric machines and other Litz wire applications, especially at cryo-temperatures down to 25 K. It is worth mentioning that the achievement of the lowest Al Litz losses depends on the balance between DC and eddy current losses, which involves the combination of material properties and operational temperatures and will be detailed in a following publication.

REFERENCES

[1] (2021). *GKN Aerospace Leads the Development of a Ground-Breaking Hydrogen Propulsion System for Aircraft*. Accessed: Jan. 27, 2021. [Online]. Available: https://www.gknaerospace.com/news-insights/news/gkn-aerospace-leads-development-of-ground-breaking-hydrogen-propulsion-system-for-aircraft/

[2] M. D. Sumption, J. Murphy, M. Susner, and T. Haugan, ''Performance metrics of electrical conductors for aerospace cryogenic motors, generators, and transmission cables,'' *Cryogenics*, vol. 111, Oct. 2020, Art. no. 103171.

[3] F. Marignetti and G. Rubino, ''Perspectives on electric machines with cryogenic cooling,'' *Energies*, vol. 16, no. 7, p. 2994, Mar. 2023.

[4] H. Schefer, W.-R. Canders, J. Hoffmann, R. Mallwitz, and M. Henke, ''Cryogenically-cooled power electronics for long-distance aircraft,'' *IEEE Access*, vol. 10, pp. 133279–133308, 2022.

[5] L. F. D. Bucho, J. F. P. Fernandes, M. Biasion, S. Vaschetto, and A. Cavagnino, ''Experimental assessment of cryogenic cooling impact on induction motors,'' *IEEE Trans. Energy Convers.*, vol. 37, no. 4, pp. 2629–2636, Dec. 2022.

[6] M. Biasion, I. S. P. Peixoto, J. F. P. Fernandes, S. Vaschetto, G. Bramerdorfer, and A. Cavagnino, ''Iron loss characterization in laminated cores at room and liquid nitrogen temperature,'' in *Proc. IEEE Energy Convers. Congr. Expo. (ECCE)*, Detroit, MI, USA, Oct. 2022, pp. 1–8.

[7] M. Biasion, F. P. J. Fernandes, P. J. D. C. Branco, S. Vaschetto, A. Cavagnino, and A. Tenconi, ''A comparison of cryogenic-cooled and superconducting electrical machines,'' in *Proc. IEEE Energy Convers. Congr. Expo. (ECCE)*, Vancouver, BC, Canada, Oct. 2021, pp. 4045–4052.

[8] H. Zhang, Z. Wen, F. Grilli, K. Gyftakis, and M. Mueller, ''Alternating current loss of superconductors applied to superconducting electrical machines,'' *Energies*, vol. 14, no. 8, p. 2234, Apr. 2021.

[9] C. Hartmann, J. K. Nøland, R. Nilssen, and R. Mellerud, ''Dual use of liquid hydrogen in a next-generation PEMFC-powered regional aircraft with superconducting propulsion,'' *IEEE Trans. Transport. Electrific.*, vol. 8, no. 4, pp. 4760–4778, Dec. 2022.

[10] F. Weng, M. Zhang, A. Elwakeel, T. Lan, N. McNeill, and W. Yuan, ''Transient test and AC loss study of a cryogenic propulsion unit for all electric aircraft,'' *IEEE Access*, vol. 9, pp. 59628–59636, 2021.

[11] H. Zhang, K. Kails, P. Machura, and M. Mueller, ''Conceptual design of electrodynamic wheels based on HTS Halbach array magnets,'' *IEEE Trans. Appl. Supercond.*, vol. 31, no. 5, pp. 1–6, Aug. 2021.

[12] L. Zheng, T. X. Wu, D. Acharya, K. B. Sundaram, J. Vaidya, L. Zhao, L. Zhou, C. H. Ham, N. Arakere, J. Kapat, and L. Chow, ''Design of a superhigh-speed cryogenic permanent magnet synchronous motor,'' *IEEE Trans. Magn.*, vol. 41, no. 10, pp. 3823–3825, Oct. 2005.

[13] F. Marignetti, S. Carbone, V. Delli Colli, and C. Attaianese, ''Cryogenic characterization of copper-wound linear tubular actuators,'' *IEEE Trans. Ind. Electron.*, vol. 59, no. 5, pp. 2167–2177, May 2012.

[14] H. M. Kim, K. W. Lee, D. G. Kim, J. H. Park, and G. S. Park, ''Design of cryogenic induction motor submerged in liquefied natural gas,'' *IEEE Trans. Magn.*, vol. 54, no. 3, pp. 1–4, Mar. 2018.

[15] H. Hoshikawa, I. Tanaka, and T. Megumi, ''Refining technology and low temperature properties for high purity aluminum,'' Sumitomo Kagaku, Tokyo, Japan, Tech. Rep., 2013, pp. 1–12. [Online]. Available: https://www.sumitomo-chem.co.jp/english/rd/report/files/docs/2013E_2.pdf

[16] D. J. Scott, R. M. Calfo, and H. R. Schwenk, ''Development of high power density pulsed AC generator,'' in *Proc. 8th IEEE Int. Conf. Pulsed Power*, San Diego, CA, USA, Jun. 1991, pp. 549–552.

[17] D. Filusch, M. Breiteneder, and H.-G. Herzog, ''Design of a hyperconducting synchronous machine for high-torque applications,'' in *Proc. 13th Int. Conf. Electr. Mach. (ICEM)*, Alexandroupoli, Greece, Sep. 2018, pp. 2092–2098.

[18] J. Lyu, H. C. Chen, Y. Zhang, Y. Du, and Q. S. Cheng, ''Litz wire and uninsulated twisted wire assessment using a multilevel PEEC method,'' *IEEE Trans. Power Electron.*, vol. 37, no. 2, pp. 2372–2381, Feb. 2022.

[19] M. A. Bakar, M. F. Alam, and K. Bertilsson, ''Modeling and characterization of series connected hybrid transformers for low-profile power converters,'' *IEEE Access*, vol. 8, pp. 53293–53306, 2020.

[20] A. Triviño, J. Sánchez, and A. Delgado, ''Efficient methodology of the coil design for a dynamic wireless charger,'' *IEEE Access*, vol. 10, pp. 83368–83378, 2022.

[21] Q. Deng, J. Liu, D. Czarkowski, M. K. Kazimierczuk, M. Bojarski, H. Zhou, and W. Hu, ''Frequency-dependent resistance of litz-wire square solenoid coils and quality factor optimization for wireless power transfer,'' *IEEE Trans. Ind. Electron.*, vol. 63, no. 5, pp. 2825–2837, May 2016.

[22] J. Zhang, H. Jiang, Z. Zhang, L. Yu, and X. Zhu, ''AC loss analytic method and optimization of litz winding for high-speed electrical machines,'' *IEEE Trans. Ind. Electron.*, vol. 71, no. 4, pp. 3330–3341, Apr. 2024, doi: 10.1109/TIE.2023.3277127.

[23] A. Selema, M. Gulec, M. N. Ibrahim, R. Sprangers, and P. Sergeant, ''Selection of magnet wire topologies with reduced AC losses for the windings of electric drivetrains,'' *IEEE Access*, vol. 10, pp. 121531–121546, 2022.

[24] G.-Y. Zhou, T.-W. Zhou, G. Ombach, X. Gong, Y.-C. Wang, and J.-X. Shen, ''Measurement of proximity losses in litz wires,'' in *Proc. IEEE Student Conf. Electric Mach. Syst.*, Huzhou, China, Dec. 2018, pp. 1–5.

[25] H. Rossmanith, M. Doebroenti, M. Albach, and D. Exner, ''Measurement and characterization of high frequency losses in nonideal litz wires,'' *IEEE Trans. Power Electron.*, vol. 26, no. 11, pp. 3386–3394, Nov. 2011.

[26] C. D. Manolopoulos, M. F. Iacchetti, A. C. Smith, P. Miller, and M. Husband, ''Litz wire loss performance and optimization for cryogenic windings,'' *IET Electr. Power Appl.*, vol. 17, no. 4, pp. 487–498, Apr. 2023.

[27] A. Tessarolo, ''Leakage field analytical computation in semiclosed slots of unsaturated electric machines,'' *IEEE Trans. Energy Convers.*, vol. 30, no. 2, pp. 431–440, Jun. 2015.

[28] C. R. Sullivan and R. Y. Zhang, ''Analytical model for effects of twisting on litz-wire losses,'' in *Proc. IEEE 15th Workshop Control Model. Power Electron. (COMPEL)*, Santander, Spain, Jun. 2014, pp. 1–10.

[29] J. A. Ferreira, ''Improved analytical modeling of conductive losses in magnetic components,'' *IEEE Trans. Power Electron.*, vol. 9, no. 1, pp. 127–131, Jan. 1994.

[30] J. Gyselinck and P. Dular, ''Frequency-domain homogenization of bundles of wires in 2-D magnetodynamic FE calculations,'' *IEEE Trans. Magn.*, vol. 41, no. 5, pp. 1416–1419, May 2005.

[31] D. C. Meeker. *Effective Material Properties of Wound Coils From an Equivalent Foil Approach*. Accessed: Dec. 28, 2006. [Online]. Available: http://www.femm.info/examples/prox/notes.pdf

[32] D. C. Meeker, ''An improved continuum skin and proximity effect model for hexagonally packed wires,'' *J. Comput. Appl. Math.*, vol. 236, no. 18, pp. 4635–4644, Dec. 2012.

[33] J. G. Hust and A. B. Lankford, ''Thermal conductivity of aluminum, copper, iron, and tungsten for temperatures from 1 K to the melting point,'' U.S. Dept. Commerce, Nat. Bur. Standards, Boulder, CO, USA, Tech. Rep., 1984. [Online]. Available: https://nvlpubs.nist.gov/nistpubs/Legacy/IR/nbsir84-3007.pdf, doi: 10.6028/NBS.IR.84-3007.

[34] C. Manolopoulos, ''Superconducting machines for aerospace electric propulsion systems,'' Ph.D. thesis, Dept. Elect. Electron. Eng., Univ. Manchester, Manchester, U.K., 2019.

[35] B. Jankowski, D. Kapelski, M. Karbowiak, M. Przybylski, and B. Ślusarek, ''Influence of cryogenic temperature on magnetic properties of soft magnetic composites,'' *Powder Metall.*, vol. 57, no. 2, pp. 155–160, Apr. 2014.

[36] D. Kapelski, B. Jankowski, M. Przybylski, and B. S´lusarek, ''The influence of the temperature of liquid nitrogen on the physical properties of powder magnetic composites,'' *Arch. Metall. Mater.*, vol. 60, no. 2, pp. 1323–1326, Jun. 2015.

[37] G. Bertotti, ''General properties of power losses in soft ferromagnetic materials,'' *IEEE Trans. Magn.*, vol. MAG-24, no. 1, pp. 621–630, Jan. 1988.

HONGYE ZHANG (Member, IEEE) received the B.Sc. and M.Sc. degrees in electrical engineering from Xi'an Jiaotong University, Xi'an, China, in 2015 and 2018, respectively, the Diplôme d'Ingénieur degree from École Centrale de Lyon, Écully, France, in 2018, and the Ph.D. degree in applied superconductivity from The University of Edinburgh, Edinburgh, U.K., in 2021. From 2021 to 2024, he was a Research Associate with The University of Manchester, Manchester, U.K., working on the £54 million H2GEAR Program to accelerate zero emission aerospace. He is currently a Lecturer (Assistant Professor) in superconducting/cryogenic electric machines with The University of Edinburgh and a Visiting Research Fellow with The University of Manchester. His research interests include modeling and testing of high temperature superconductors, design and analysis of cryogenic/superconducting machines, and application of hydrogen energy.

MATTEO F. IACCHETTI (Senior Member, IEEE) received the Ph.D. degree in electrical engineering from Politecnico di Milano, Milan, Italy, in 2008. In 2014, he joined the Department of Electrical and Electronic Engineering, The University of Manchester, Manchester, U.K., where he is currently a Senior Lecturer. Since 2021, he has been an Associate Professor with the Department of Energy, Politecnico di Milano. His main research interests include the design, modeling, and control of electric machines for propulsion, and cryogenic electric motors.

ALEXANDER C. (SANDY) SMITH (Senior Member, IEEE) received the B.Sc. (Eng.) and Ph.D. degrees from Aberdeen University, U.K., in 1977 and 1980, respectively. His previous academic appointments was with Imperial College London and the University of Cambridge. He joined Invensys Brook Crompton, as the Head of Research for Motor Technology, in 1997. He is currently a Professor of electrical machines with The University of Manchester and the Director of the Roll-Royce University Technology Centre on Electrical Systems for Extreme Environments. His research interests include the design and modeling of motors, generators, superconducting machines, and electrical drive systems. He is a fellow of the Institute of Engineering and Technology. He is the Editor-in-Chief of the *IET Electrical Systems in Transportation*.

PAUL M. TUOHY received the B.Eng. degree (Hons.) in mechatronics with industrial experience and the Ph.D. degree in electrical engineering from The University of Manchester, Manchester, U.K., in 2006 and 2011, respectively. He is currently a Research Fellow with The University of Manchester. His research interests include the design, finite element analysis (FEA), optimization, and testing of electric machines, actuators, and drives for aerospace, electric vehicle, marine, and renewable energy applications. He was a recipient of the Siemens Medal, in 2006. He was elected Whitworth Scholar, in 2007, and the Whitworth Senior Scholar, in 2012.

CHARALAMPOS D. MANOLOPOULOS received the Diploma degree in electrical and computer engineering from the Aristotle University of Thessaloniki, Greece, in 2011, and the M.Sc. and Ph.D. degrees in electrical engineering from The University of Manchester, U.K., in 2014 and 2019, respectively. After a short period as a Research Associate with The University of Manchester, he joined GKN Aerospace, Bristol, U.K., in 2020. His main research interests include the design and modeling of electrical machines, and cryogenic electric motors.

ALEXANDRU-VLAD RUSU received the B.Eng. degree in electrical and electronic engineering from The University of Manchester, Manchester, U.K., in 2020, where he is currently pursuing the Ph.D. degree researching high-power density electrical machines for aerospace applications. His main research interests include the modeling and design of conventional and cryogenic electrical machines.

VICENTE CLIMENTE-ALARCON (Senior Member, IEEE) received the M.Sc. degrees in chemical and industrial engineering and the Ph.D. degree in electrical engineering from Universitat Politècnica de València, Valencia, Spain, in 2000, 2011, and 2012, respectively. He was an Adjunct Professor with the School of Industrial Engineering, Universitat Politècnica de València, working on condition monitoring of electrical machines. In 2014, he moved to Finland to carry out postdoctoral research with the Department of Electrical Engineering and Automation, Aalto University, in multiphysics simulation of electrical machines. In 2018, he joined the Department of Materials Science and Metallurgy, University of Cambridge, where he contributed to the development of a fully superconducting motor. Since 2020, he has been with GKN Aerospace developing cryogenic motors for aircraft propulsion within the H2GEAR Program.